http://communications.science.ankara.edu.tr

Commun.Fac.Sci.Univ.Ank.Ser. A1 Math. Stat.
Volume 73, Number 4, Pages 1171–1196 (2024)
DOI:10.31801/cfsuasmas.1475286
ISSN 1303-5991 E-ISSN 2618-6470

Research Article; Received: April 29, 2024; Accepted: September 19, 2024

THE DEPENDENCY OF THE ANALYTICAL AND NUMERICAL SOLUTION ON THE ε PARAMETER IN HYPERBOLIC AND PSEUDO-HYPERBOLIC PROBLEMS WITH INVERSE COEFFICIENTS

Akbala YERNAZAR[1], Erman ASLAN[2], İrem BAĞLAN[3]

[1,3]Department of Mathematics, Kocaeli University, Kocaeli, TÜRKİYE
[2]Department of Mechanical Engineering, Kocaeli University, Kocaeli, TÜRKİYE

Abstract. The aim of this study is to analyze the behavior of ε on the solution of an inverse coefficient nonlinear pseudo-hyperbolic equation $\omega_{tt}-\varepsilon\omega_{xxtt}-\omega_{xx}=\theta(t)f(x,t,\omega)$ with periodic boundary conditions. We also consider the inverse coefficient problem $\omega_{tt}-\omega_{xx}=\theta(t)f(x,t,\omega)$. The solution function of nonlinear pseudo-hyperbolic equation is found to be convergent to the solution function of nonlinear hyperbolic equation, when $\varepsilon\to 0$ is proved. The Fourier method was used to illustrate the theoretically relation between the inverse problems while the Finite Difference Method was used numerically. In order to get more accurate numerical solution higher precision schemes have been applied in implicit finite difference equation. The cases where $\varepsilon=0$ and $\varepsilon\neq 0$ have been solved analytically and numerically, and compared each other.

1. Introduction

Nonlinear hyperbolic equations and nonlinear pseudo-hyperbolic equations are both types of partial differential equations (PDEs) that arise in various areas of physics and engineering. While they share some similarities, they have distinct characteristics.

2020 *Mathematics Subject Classification.* 35R30.

Keywords. Nonlinear pseudo-hyperbolic equation, inverse coefficient problem, periodic boundary condition, Fourier method, finite difference method.

[1] akbala.yernazar@kocaeli.edu.tr; 0000-0002-0068-4954;
[2] erman.aslan@kocaeli.edu.tr-Corresponding author; 0000-0001-8595-6092;
[3] isakinc@kocaeli.edu.tr; 0000-0002-1877-9791.

©2024 Ankara University
Communications Faculty of Sciences University of Ankara Series A1 Mathematics and Statistics

Hyperbolic equations typically describe wave phenomena, where information propagates along characteristics at finite speed [24]. In the nonlinear case, the coefficients and/or terms n the equation are nonlinear functions of the dependent variable. Examples of nonlinear hyperbolic equations include the nonlinear wave equation [21, 35], the Euler equations for compressible fluid flow [27, 39], and the nonlinear acoustics equations [30].

Pseudo-hyperbolic equations also describe wave-like behavior, but they may not exhibit strict characteristics along which information propagates. They often arise as generalizations of hyperbolic equations or in systems where certain terms introduce dispersive effects or alter the characteristics of wave propagation [19]. Nonlinear pseudo-hyperbolic equations can involve terms with mixed spatial and temporal derivatives and can exhibit dispersive or diffusive behavior alongside wave-like propagation. Examples include certain models of viscoelasticity [29], nonlinear versions of the Korteweg–de Vries equation [22], and some models in nonlinear optics.

In summary, while both types of equations describe wave-like phenomena, nonlinear hyperbolic equations typically follow characteristics along which information propagates at finite speed, while nonlinear pseudo-hyperbolic equations may exhibit dispersive effects or altered wave propagation behavior due to the presence of certain terms.

Numerous analytical techniques exist for solving differential equations. Nonetheless, detecting arbitrary functions that fulfill given boundary conditions within these equations can pose challenges. In fact, finding the general solution of partial differential equations is generally impossible except in specific scenarios. Consequently, various approaches have been devised for addressing boundary value problems. Among these, the Fourier method stands out as a well-known technique, relying on the separation of variables [5].

The study of inverse problems emerged in the 19th and 20th centuries, contributing to the resolution of numerous challenges in heat transfer, diffusion, nuclear physics, seismology. Inverse problems can be utilized with parabolic equations [6-8, 17, 28]. In addition, inverse problems can also be used for hyperbolic and/or pseudo hyperbolic equations [9, 25, 31, 32].

The present investigation employs the periodic boundary condition, which is a specific instance of the nonlocal boundary condition [1]. Periodic boundary condition is combination between Dirichlet (giving constant properties) and Neumann (giving constant flux) boundary conditions, and it generally utilizes to avoid large computational domains for numerical and analytical computation [3, 4].

For the numerical solution of one-dimensional wave equations with inverse coefficients (hyperbolic and pseudo-hyperbolic), there are several numerical methods, which are finite difference method [23, 34], finite element method [11-13], and finite volume method [10, 14-16, 20, 36, 37], available. There are many studs that solve the wave equation (hyperbolic and/or pseudo hyperbolic equations) using the finite difference method [2, 33, 38].

In the present study, we investigate an inverse problem of unknown time-dependent coefficients in the one-dimensional nonlinear hyperbolic and/or pseudo equation with periodic boundary conditions. For an analytical solution, the Fourier method is utilized to generate Fourier coefficients for the solutions, and through an iterative approach, we establish the convergence, uniqueness, and stability of the solution to the nonlinear problem. For numerical solution, implicit finite difference scheme is utilized. To achieve a more accurate solution, higher precision schemes have been employed in implicit finite difference equation. A second-order accurate time discretization is implemented, and fourth-order accurate finite difference equations are utilized for the discretization of spatial and multi-variable partial differential equations. The cases where epsilon equals 0 and epsilon not equal to 0 (different epsilon values) have been solved analytically and numerically, and compared with each other.

2. Solution of the Problems

Here, we studied mixed problems of two physical phenomena models: pseudo-hyperbolic equation (1) and hyperbolic equation (5) in the domain $(x,t) \in \Omega\,(0 < x < \pi,\, 0 < t < T)$:

$$\tilde{\omega}_{tt} - \varepsilon\tilde{\omega}_{xxtt} - \tilde{\omega}_{xx} = \tilde{\theta}(t) f(x,t,\tilde{\omega}), \tag{1}$$

$$\begin{aligned} \tilde{\omega}(x,0,\varepsilon) &= \chi(x), \\ \tilde{\omega}_t(x,0,\varepsilon) &= \phi(x), \end{aligned} \tag{2}$$

$$\begin{aligned} \tilde{\omega}(x,0,\varepsilon) &= \chi(x), \\ \tilde{\omega}_t(x,0,\varepsilon) &= \phi(x), \end{aligned} \tag{3}$$

$$\tilde{E}(t,\varepsilon) = \int_0^{\pi} x\tilde{\omega}(x,t,\varepsilon)dx. \tag{4}$$

The initial, boundary, and overdetermination conditions of the pseudo-hyperbolic equation are illustrated by (2), (3), and (4), respectively. Similarly, the initial and boundary conditions set for the solutions of the hyperbolic equation (5) expressed as follows:

$$\omega_{tt} - \omega_{xx} = \theta(t) f(x,t,\omega), \tag{5}$$

$$\begin{aligned} \omega(x,0) &= \chi(x), \\ \omega_t(x,0) &= \phi(x), \end{aligned} \tag{6}$$

$$\begin{aligned} \omega(0,t) &= \omega(\pi,t), \\ \omega_x(0,t) &= \omega_x(\pi,t), \end{aligned} \tag{7}$$

$$E(t) = \int_0^{\pi} x\omega(x,t)dx. \tag{8}$$

Equation (5) is obtained from (1) by setting $\varepsilon = 0$. Here, the equation simplifies to the standard wave equation. This describes classical wave phenomena where the speed of wave propagation is constant and there is no additional dependence on mixed spatial and temporal derivatives. Where $\varepsilon \geq 0$ is a small parameter, $\chi(x)$, $\phi(x)$ and $E(t,\varepsilon)$ are given functions on $x \in (0,\pi)$ and $t \in (0,T)$, respectively. Here, the term $\varepsilon\tilde{\omega}_{xxtt}$ introduces a damping-like or dispersive effect. This term can account for additional physical phenomena like viscosity or diffusive effects, leading to modified wave propagation characteristics. For example, it can model how waves interact with a medium that has additional resistance or how they spread out over time.

In [18, 26], the authors analyzed the dependence of the solution of direct problems on ε. In this paper, we show the dependence of the solution of inverse coefficient problems on ε; that is, the solution function $\tilde{\omega}(x,t,\varepsilon)$ of (1)-(4) is convergent to the solution function $\omega(x,t)$ of (5)-(8) as $\varepsilon \to 0$.

In mathematical physics, direct problems aim to find functions that describe physical processes, such as sound or heat propagation. Inverse problems arise when the properties of the medium are unknown and it is necessary to determine these properties based on information about the solution of the direct problem.

Definition 1. *In the inverse problem, in addition to $\omega(x,t)$, there is unknown of function included in the direct problem. This unknown pair $\{\theta(t),\, \omega(x,t)\}$ is called the solution of the inverse problem.*

Definition 2. *Banach space is a space in which there exists a set of continuous functions on $[0,T]$, denoted by $\{\omega(t)\} = \{\omega_0(t),\, \omega_{ck}(t),\, \omega_{sk}(t),\ k \in N\}$, that satisfy the norm*

$$\|\omega(t)\| = \max_{0\leq t\leq T} |\omega_0(t)| + \sum_{k=1}^{\infty} \left(\max_{0\leq t\leq T} |\omega_{ck}(t)| + \max_{0\leq t\leq T} |\omega_{sk}(t)| \right).$$

Here, we seek a general solution to (1)-(4) as in

$$\tilde{\omega}(x,t) = \frac{\tilde{\omega}_0}{2} + \sum_{k=1}^{\infty} [\tilde{\omega}_{ck}(x,t)\cos 2kx + \tilde{\omega}_{sk}(x,t)\sin 2kx].$$

The solution obtained is denoted by (9) below

$$\begin{aligned} \tilde{\omega}(x,t,\varepsilon) =& \frac{1}{2}\left(\chi_0 + \phi_0 t + \frac{2}{\pi}\int_0^t\int_0^\pi \tilde{\theta}(\tau)(t-\tau) f(\xi,\tau,\tilde{\omega})d\xi d\tau \right) \\ &+ \sum_{k=1}^{\infty}\left(\chi_{ck}\cos\tilde{\alpha}_k t + \frac{1}{\tilde{\lambda}_k}\phi_{ck}\sin\tilde{\alpha}_k t \right. \\ &\left. + \frac{1}{\tilde{\lambda}_k}\frac{2}{\pi}\int_0^t\int_0^\pi \tilde{\theta}(\tau) f(\xi,\tau,\tilde{\omega})\cos 2k\xi \sin\tilde{\lambda}_k(t-\tau)d\xi d\tau \right)\cos 2kx \end{aligned} \tag{9}$$

$$+\sum_{k=1}^{\infty}\left(\chi_{sk}\cos\tilde{\alpha}_k t+\frac{1}{\tilde{\lambda}_k}\phi_{sk}\sin\tilde{\alpha}_k t\right.$$
$$\left.+\frac{1}{\tilde{\lambda}_k}\frac{2}{\pi}\int_0^t\int_0^\pi\tilde{\theta}(\tau)f(\xi,\tau,\tilde{\omega})\sin 2k\xi\sin\tilde{\lambda}_k(t-\tau)d\xi d\tau\right)\sin 2kx,$$

$\tilde{\lambda}_k=\frac{2k}{\sqrt{1+4\varepsilon k^2}},\ k=\overline{1,\infty}$.

By multiplying equation (1) by x and integrating it over the interval $[0,\pi]$, and using initial data (2) and overdetermination condition (4), we find

$$\tilde{\theta}(t)=\frac{\tilde{E}''(t)+\varepsilon\phi_t(\pi)-\varepsilon\phi_t(0)}{\int_0^\pi xf(x,t,\tilde{\omega})dx}$$
$$-\frac{\pi\sum_{k=1}^{\infty}(2k)\left\{\left(1-\varepsilon\tilde{\lambda}_k^2\right)\chi_{sk}\cos\tilde{\lambda}_k t+\left(\frac{1}{\tilde{\lambda}_k}-\varepsilon\tilde{\lambda}_k\right)\phi_{sk}\sin\tilde{\lambda}_k t+\frac{1}{\tilde{\lambda}_k}\frac{2}{\pi}\int_0^t\int_0^\pi\tilde{\theta}(\tau)f(\xi,\tau,\tilde{\omega})\sin 2k\xi\sin\tilde{\lambda}_k(t-\tau)d\xi d\tau\right\}}{\int_0^\pi xf(x,t,\tilde{\omega})dx}. \tag{10}$$

We seek a general solution to equations (5)-(8) as in

$$\omega(x,t)=\frac{\omega_0}{2}+\sum_{k=1}^{\infty}[\omega_{ck}(x,t)\cos 2kx+\omega_{sk}(x,t)\sin 2kx],$$

and we find the solution

$$\omega(x,t)=\frac{1}{2}\left(\chi_0+\phi_0 t+\frac{2}{\pi}\int_0^t\int_0^\pi\theta(\tau)(t-\tau)f(\xi,\tau,\omega)d\xi d\tau\right)$$
$$+\sum_{k=1}^{\infty}\left(\chi_{ck}\cos\lambda_k t+\frac{\phi_{ck}}{2k}\sin\lambda_k t\right.$$
$$\left.+\frac{1}{\alpha_k}\int_0^t\int_0^\pi\theta(\tau)f(\xi,\tau,\omega)\cos 2k\xi\sin\lambda_k(t-\tau)d\xi d\tau\right)\cos 2kt \tag{11}$$
$$+\sum_{k=1}^{\infty}\left(\chi_{sk}\cos\lambda_k t+\frac{\phi_{sk}}{2k}\sin\lambda_k t\right.$$
$$\left.+\frac{1}{\alpha_k}\int_0^t\int_0^\pi\theta(\tau)f(\xi,\tau,\omega)\sin 2k\xi\sin\lambda_k(t-\tau)d\xi d\tau\right)\sin 2k,$$

$\lambda_k = 2k,\ k = \overline{1,\infty}$.

With the same method we obtained an inverse coefficient to (5)-(8) as following;

$$\theta(t) = \frac{E''(t) - \pi \sum\limits_{k=1}^{\infty} (2k) \left(\chi_{sk} \cos \lambda_k t + \frac{\phi_{sk}}{2k} \sin \lambda_k t + \frac{1}{2k} \int_0^t \theta(\tau) f_{sk}(\tau) \sin \lambda_k (t-\tau) d\tau \right)}{\int_0^{\pi} x f(x,t,\omega) dx}. \tag{12}$$

3. Analysis of Convergence of Solutions

Theorem 1. *If following*
1.$E(t) \in C^2[0,T],\ \theta(t) \in C[0,T]$.
2.$\varphi(x) \in C^1[0,\pi],\ \psi(x) \in C^1[0,\pi]$.
3.The function $f(x,t,\omega)$ *be continuous to all arguments in* $\Omega \times (-\infty,\infty)$ *and satisfies the following conditions*
i) $\left| \frac{\partial^{(s)} f(x,t,\omega)}{\partial x^{(s)}} - \frac{\partial^{(s)} f(x,t,\tilde{\omega})}{\partial x^{(s)}} \right| \le b(x,t) \left| \omega - \tilde{\omega} \right|,\ s = \overline{0,2}$,
$b(x,t) \in L_2(D),\ b(x,t) \ge 0$;
ii) $f(x,t,\omega) \in C^1[0,\ \pi],\ |f(x,t,\omega)| \le M,\ t \in [0,\ T]$;
iii) $\int_0^{\pi} f(x,t,\omega) dx \ne 0,\ \forall t \in [0,T]$ *conditions are fulfilled, then*
$\lim\limits_{\varepsilon \to 0} \tilde{\omega}(x,t,\varepsilon) = \omega(x,t)$.

Proof. Firstly, we examine the difference of the time dependent coefficiets (10) and (12) and as follows;

$$\tilde{\theta}(t) - \theta(t) = \frac{\tilde{E}''(t) + \varepsilon \phi_t(\pi) - \varepsilon \phi_t(0)}{\int\limits_0^{\pi} x f(x,t,\tilde{\omega}) dx}$$

$$- \frac{\pi \sum\limits_{k=1}^{\infty} \left\{ a_k \chi'_{ck} \cos \tilde{\lambda}_k t + b_k \phi_{sk} \sin \tilde{\lambda}_k t + \frac{1}{\tilde{\lambda}_k} \frac{2}{\pi} \int\limits_0^t \int\limits_0^{\pi} \tilde{\theta}(\tau) f'(\xi,\tau,\tilde{\omega}) \cos 2k\xi \sin \tilde{\lambda}_k (t-\tau) d\xi d\tau \right\}}{\int\limits_0^{\pi} x f(x,t,\tilde{\omega}) dx}$$

$$- \frac{E''(t) - \pi \sum\limits_{k=1}^{\infty} \left(\chi'_{sk} \cos \lambda_k t + \phi_{sk} \sin \lambda_k t + \frac{1}{\lambda_k} \frac{2}{\pi} \int\limits_0^t \int\limits_0^{\pi} \theta(\tau) f'(\xi,\tau,\omega) \cos 2k\xi \sin \lambda_k (t-\tau) d\xi d\tau \right)}{\int_0^{\pi} x f(x,t,\omega) dx},$$

$a_k = \frac{1}{1+4\varepsilon k^2}$, $b_k = \frac{1}{\sqrt{1+4\varepsilon k^2}}$. Then we have

$$\tilde{\theta}(t) - \theta(t) = \frac{2}{\pi^2 M_*} \left(\tilde{E}''(t) - E''(t) \right) + \frac{2}{\pi^2 M_*} \left(\varepsilon \phi_t(\pi) - \varepsilon \phi_t(0) \right)$$

$$+\frac{2}{\pi M_*}\sum_{k=1}^{\infty}\chi'_{ck}\left(\cos\lambda_k t-a_k\cos\tilde{\lambda}_k t\right)+\frac{2}{\pi M_*}\sum_{k=1}^{\infty}\phi_{sk}\left(\sin\lambda_k t-b_k\sin\tilde{\lambda}_k t\right)$$
$$+\frac{2}{\pi M_*}\sum_{k=1}^{\infty}\left(\frac{1}{\lambda_k}\frac{2}{\pi}\int_0^t\int_0^\pi\theta(\tau)f'(\xi,\tau,\omega)\cos 2k\xi\sin\lambda_k(t-\tau)d\xi d\tau\right.$$
$$\left.-\frac{1}{\tilde{\lambda}_k}\frac{2}{\pi}\int_0^t\int_0^\pi\tilde{\theta}(\tau)f'(\xi,\tau,\tilde{\omega})\cos 2k\xi\sin\tilde{\lambda}_k(t-\tau)d\xi d\tau\right).$$

If the absolute value of the difference is taken after adding and subtracting and making the necessary grouping, we have

$$\begin{aligned}\left|\tilde{\theta}(t)-\theta(t)\right|\leq&\frac{2}{\pi^2 M_*}\left|\tilde{E}''(t)-E''(t)\right|+\frac{2}{\pi^2 M_*}\left|\varepsilon\phi_t(\pi)-\varepsilon\phi_t(0)\right|\\&+\frac{2}{\pi M_*}\sum_{k=1}^{\infty}\left|\chi'_{ck}\right|\left|\cos\lambda_k t-a_k\cos\tilde{\lambda}_k t\right|+\frac{2}{\pi M_*}\sum_{k=1}^{\infty}\left|\phi_{sk}\right|\left|\sin\lambda_k t-b_k\sin\tilde{\lambda}_k t\right|\\&+\frac{2}{\pi M_*}\sum_{k=1}^{\infty}\frac{1}{\lambda_k}\frac{2}{\pi}\left|\int_0^t\int_0^\pi\left[\tilde{\theta}(t)-\theta(t)\right]f'(\xi,\tau,\omega)\cos 2k\xi\sin\lambda_k(t-\tau)d\xi d\tau\right|\\&+\frac{2}{\pi M_*}\sum_{k=1}^{\infty}\left|\frac{1}{\lambda_k}-\frac{1}{\tilde{\lambda}_k}\right|\frac{2}{\pi}\left|\int_0^t\int_0^\pi\tilde{\theta}(\tau)f'(\xi,\tau,\tilde{\omega})\cos 2k\xi\sin\tilde{\lambda}_k(t-\tau)d\xi d\tau\right|\\&+\frac{2}{\pi M_*}\sum_{k=1}^{\infty}\frac{1}{\lambda_k}\frac{2}{\pi}\left|\int_0^t\int_0^\pi\tilde{\theta}(\tau)\left[f'(\xi,\tau,\tilde{\omega})-f'(\xi,\tau,\omega)\right]\cos 2k\xi\sin\lambda_k(t-\tau)d\xi d\tau\right|\\&+\frac{2}{\pi M_*}\sum_{k=1}^{\infty}\frac{1}{\lambda_k}\int_0^t\left(\frac{2}{\pi}\left|\int_0^\pi\tilde{\theta}(\tau)f'(\xi,\tau,\tilde{\omega})\cos 2k\xi d\xi\right|\right)\left|\sin\lambda_k(t-\tau)-\sin\tilde{\lambda}_k(t-\tau)\right|d\tau.\end{aligned}\tag{13}$$

From (13), the statements $\left|\tilde{E}''(t)-E''(t)\right|$, $\left|\varepsilon\phi_t(\pi)-\varepsilon\phi_t(0)\right|$, $\left|\frac{1}{\lambda_k}-\frac{1}{\tilde{\lambda}_k}\right|$, $\left|\sin\lambda_k t-b_k\sin\tilde{\lambda}_k t\right|$, $\left|\cos\lambda_k t-a_k\cos\tilde{\lambda}_k t\right|$, $\left|\sin\lambda_k(t-\tau)-\sin\tilde{\lambda}_k(t-\tau)\right|$ are bounded for k, τ and t $(0\leq\tau\leq t\leq T)$ as $\varepsilon\to 0$, also a_k, b_k are limited. Let us denote all of these statements by $\sigma(\varepsilon)$ and we rewrite (13) as following

$$\left|\tilde{\theta}(t)-\theta(t)\right|\leq\sigma(\varepsilon)+\frac{2}{\pi M_*}\sum_{k=1}^{\infty}\frac{1}{\tilde{\lambda}_k}\frac{2}{\pi}\left|\int_0^t\int_0^\pi\left[\tilde{\theta}(\tau)-\theta(\tau)\right]f'(\xi,\tau,\omega)\cos 2k\xi\sin\lambda_k(t-\tau)d\xi d\tau\right|$$

$$+\frac{2}{\pi M_*}\sum_{k=1}^{\infty}\frac{1}{\lambda_k}\frac{2}{\pi}\left|\int_0^t\int_0^\pi \tilde{\theta}(\tau)\left[f'(\xi,\tau,\tilde{\omega})-f'(\xi,\tau,\omega)\right]\cos 2k\xi\sin\lambda_k(t-\tau)d\xi d\tau\right|.$$

Applying Cauchy, Bessel, Hölder inequalities to the inequality above, we have

$$\left|\tilde{\theta}(t)-\theta(t)\right|\le\frac{\sigma(\varepsilon)}{B}+\frac{2}{BM_*}\sqrt{\frac{t}{6\pi}}\left(\int_0^t\int_0^\pi\left\{\tilde{\theta}(\tau)b(\xi,\tau)\left|\tilde{\omega}-\omega\right|\right\}^2 d\xi d\tau\right)^{\frac{1}{2}}, \qquad (14)$$

$B=1-\frac{4M}{\pi M_*}\sqrt{\frac{t}{\pi}\left(\frac{\pi^2}{24}+\varepsilon\right)}$.
Let us take the difference of the Fourier coefficients to examine the difference of the solutions (9) and (11),

$$\tilde{\omega}_0(t,\varepsilon)-\omega_0(t)=\frac{2}{\pi}\int_0^t\int_0^\pi\tilde{\theta}(\tau)(t-\tau)f(\zeta,\tau,\tilde{\omega})d\zeta d\tau-\frac{2}{\pi}\int_0^t\int_0^\pi\theta(\tau)(t-\tau)f(\zeta,\tau,\omega)d\zeta d\tau,$$

$$\begin{aligned}\tilde{\omega}_{ck}(t,\varepsilon)-\omega_{ck}(t)=&\sum_{k=1}^{\infty}\left(\chi_{ck}\cos\tilde{\alpha}_k t-\chi_{ck}\cos\alpha_k t\right)+\sum_{k=1}^{\infty}\left(\frac{1}{\tilde{\lambda}_k}\phi_{ck}\sin\tilde{\alpha}_k t-\frac{\phi_{ck}}{\lambda_k}\sin\alpha_k t\right)\\&+\sum_{k=1}^{\infty}\left(\frac{1}{\tilde{\lambda}_k}\frac{2}{\pi}\int_0^t\int_0^\pi\tilde{\theta}(\tau)f(\zeta,\tau,\tilde{\omega})\cos 2k\zeta\sin\tilde{\lambda}_k(t-\tau)d\zeta d\tau\right.\\&\left.-\frac{1}{\lambda_k}\frac{2}{\pi}\int_0^t\int_0^\pi\theta(\tau)f(\zeta,\tau,\omega)\cos 2k\zeta\sin\lambda_k(t-\tau)d\zeta d\tau\right),\end{aligned}$$

$$\begin{aligned}\tilde{\omega}_{sk}(t,\varepsilon)-\omega_{sk}(t)=&\sum_{k=1}^{\infty}\left(\chi_{sk}\cos\tilde{\alpha}_k t-\chi_{sk}\cos\alpha_k t\right)+\sum_{k=1}^{\infty}\left(\frac{1}{\tilde{\lambda}_k}\phi_{sk}\sin\tilde{\alpha}_k t-\frac{\phi_{sk}}{\lambda_k}\sin\alpha_k t\right)\\&+\sum_{k=1}^{\infty}\left(\frac{1}{\tilde{\lambda}_k}\frac{2}{\pi}\int_0^t\int_0^\pi\tilde{\theta}(\tau)f(\zeta,\tau,\tilde{\omega})\sin 2k\zeta\sin\tilde{\lambda}_k(t-\tau)d\zeta d\tau\right.\\&\left.-\frac{1}{\lambda_k}\frac{2}{\pi}\int_0^t\int_0^\pi\theta(\tau)f(\zeta,\tau,\omega)\sin 2k\zeta\sin\lambda_k(t-\tau)d\zeta d\tau\right).\end{aligned}$$

By adding and subtracting and taking the absolute values, we obtain

$$|\tilde{\omega}_0(t,\varepsilon)-\omega_0(t)|\le\frac{2}{\pi}\left|\int_0^t\int_0^\pi\left[\tilde{\theta}(\tau)-\theta(\tau)\right](t-\tau)f(\zeta,\tau,\omega)d\zeta d\tau\right|$$

$$+\frac{2}{\pi}\left|\int_0^t\int_0^\pi \tilde{\theta}(\tau)(t-\tau)\left[f(\zeta,\tau,\tilde{\omega})-f(\zeta,\tau,\omega)\right]d\zeta d\tau\right|,$$

$$\begin{aligned}
|\tilde{\omega}_{ck}(t,\varepsilon)-\omega_{ck}(t)| \le{}& \sum_{k=1}^{\infty}|\chi_{ck}|\left|\cos\tilde{\lambda}_k t-\cos\lambda_k t\right|+\sum_{k=1}^{\infty}|\phi_{ck}|\left|\frac{\sin\tilde{\lambda}_k t}{\tilde{\lambda}_k}-\frac{\sin\lambda_k t}{\lambda_k}\right| \\
&+\sum_{k=1}^{\infty}\left|\frac{1}{\tilde{\lambda}_k}-\frac{1}{\lambda_k}\right|\frac{2}{\pi}\left|\int_0^t\int_0^\pi \tilde{\theta}(\tau)f(\zeta,\tau,\tilde{\omega})\cos 2k\zeta\sin\tilde{\lambda}_k(t-\tau)d\zeta d\tau\right| \\
&+\sum_{k=1}^{\infty}\frac{1}{\lambda_k}\frac{2}{\pi}\left|\int_0^t\int_0^\pi \left[\tilde{\theta}(\tau)-\theta(\tau)\right]f(\zeta,\tau,\tilde{\omega})\cos 2k\zeta\sin\lambda_k(t-\tau)d\zeta d\tau\right| \\
&+\sum_{k=1}^{\infty}\frac{1}{\lambda_k}\frac{2}{\pi}\left|\int_0^t\int_0^\pi \tilde{\theta}(\tau)\left[f(\zeta,\tau,\tilde{\omega})-f(\zeta,\tau,\omega)\right]\cos 2k\zeta\sin\lambda_k(t-\tau)d\zeta d\tau\right| \\
&+\sum_{k=1}^{\infty}\frac{1}{\lambda_k}\int_0^t\left(\frac{2}{\pi}\left|\int_0^\pi \tilde{\theta}(\tau)f(\zeta,\tau,\tilde{\omega})\cos 2k\zeta d\zeta\right|\right)\left|\sin\tilde{\lambda}_k(t-\tau)-\sin\lambda_k(t-\tau)\right|d\tau,
\end{aligned}$$

$$\begin{aligned}
|\tilde{\omega}_{sk}(t,\varepsilon)-\omega_{sk}(t)| \le{}& \sum_{k=1}^{\infty}|\chi_{sk}|\left|\cos\tilde{\lambda}_k t-\cos\lambda_k t\right|+\sum_{k=1}^{\infty}|\phi_{sk}|\left|\frac{\sin\tilde{\lambda}_k t}{\tilde{\lambda}_k}-\frac{\sin\lambda_k t}{\lambda_k}\right| \\
&+\sum_{k=1}^{\infty}\left|\frac{1}{\tilde{\lambda}_k}-\frac{1}{\lambda_k}\right|\frac{2}{\pi}\left|\int_0^t\int_0^\pi \tilde{\theta}(\tau)f(\zeta,\tau,\tilde{\omega})\sin 2k\zeta\sin\tilde{\lambda}_k(t-\tau)d\zeta d\tau\right| \\
&+\sum_{k=1}^{\infty}\frac{1}{\lambda_k}\frac{2}{\pi}\left|\int_0^t\int_0^\pi \left[\tilde{\theta}(\tau)-\theta(\tau)\right]f(\zeta,\tau,\tilde{\omega})\sin 2k\zeta\sin\lambda_k(t-\tau)d\zeta d\tau\right| \\
&+\sum_{k=1}^{\infty}\frac{1}{\lambda_k}\frac{2}{\pi}\left|\int_0^t\int_0^\pi \tilde{\theta}(\tau)\left[f(\zeta,\tau,\tilde{\omega})-f(\zeta,\tau,\omega)\right]\sin 2k\zeta\sin\lambda_k(t-\tau)d\zeta d\tau\right| \\
&+\sum_{k=1}^{\infty}\frac{1}{\lambda_k}\int_0^t\left(\frac{2}{\pi}\left|\int_0^\pi \tilde{\theta}(\tau)f(\zeta,\tau,\tilde{\omega})\sin 2k\zeta d\xi\right|\right)\left|\sin\tilde{\lambda}_k(t-\tau)-\sin\lambda_k(t-\tau)\right|d\tau.
\end{aligned}$$

After that, we have

$$|\tilde{\omega}(t,\varepsilon)-\omega(t)|=\frac{|\tilde{\omega}_0(t,\varepsilon)-\omega_0(t)|}{2}+\sum_{k=1}^{\infty}\left[|\tilde{\omega}_{ck}(t,\varepsilon)-\omega_{ck}(t)|+|\tilde{\omega}_{sk}(t,\varepsilon)-\omega_{sk}(t)|\right]$$

$$
\begin{aligned}
&\leq \frac{1}{\pi}\left|\int_0^t\int_0^\pi [\tilde{\theta}(\tau)-\theta(\tau)](t-\tau)f(\zeta,\tau,\omega)d\zeta d\tau\right| \\
&+\frac{1}{\pi}\left|\int_0^t\int_0^\pi \left|\tilde{\theta}(\tau)(t-\tau)\left[f(\zeta,\tau,\tilde{\omega})-f(\zeta,\tau,\omega)\right]\right| d\zeta d\tau\right| \\
&+\sum_{k=1}^{\infty}|\chi_{ck}|\left|\cos\tilde{\lambda}_k t-\cos\lambda_k t\right|+\sum_{k=1}^{\infty}|\phi_{ck}|\left|\frac{\sin\tilde{\lambda}_k t}{\tilde{\lambda}_k}-\frac{\sin\lambda_k t}{\lambda_k}\right| \\
&+\sum_{k=1}^{\infty}|\chi_{sk}|\left|\cos\tilde{\lambda}_k t-\cos\lambda_k t\right|+\sum_{k=1}^{\infty}|\phi_{sk}|\left|\frac{\sin\tilde{\lambda}_k t}{\tilde{\lambda}_k}-\frac{\sin\lambda_k t}{\lambda_k}\right| \qquad (15)\\
&+\sum_{k=1}^{\infty}\left|\frac{1}{\tilde{\lambda}_k}-\frac{1}{\lambda_k}\right|\frac{2}{\pi}\left|\int_0^t\int_0^\pi \tilde{\theta}(\tau)f(\zeta,\tau,\tilde{\omega})\cos 2k\zeta\sin\tilde{\lambda}_k(t-\tau)d\zeta d\tau\right| \\
&+\sum_{k=1}^{\infty}\frac{1}{\lambda_k}\frac{2}{\pi}\left|\int_0^t\int_0^\pi \left[\tilde{\theta}(\tau)-\theta(\tau)\right]f(\zeta,\tau,\tilde{\omega})\cos 2k\zeta\sin\lambda_k(t-\tau)d\zeta d\tau\right| \\
&+\sum_{k=1}^{\infty}\frac{1}{\lambda_k}\frac{2}{\pi}\left|\int_0^t\int_0^\pi \tilde{\theta}(\tau)\left[f(\zeta,\tau,\tilde{\omega})-f(\zeta,\tau,\omega)\right]\cos 2k\zeta\sin\lambda_k(t-\tau)d\zeta d\tau\right| \\
&+\sum_{k=1}^{\infty}\frac{1}{\lambda_k}\int_0^t\left(\frac{2}{\pi}\left|\int_0^\pi \tilde{\theta}(\tau)f(\zeta,\tau,\tilde{\omega})\cos 2k\zeta d\zeta\right|\right)\left|\sin\tilde{\lambda}_k(t-\tau)-\sin\lambda_k(t-\tau)\right| d\tau \\
&+\sum_{k=1}^{\infty}\left|\frac{1}{\tilde{\lambda}_k}-\frac{1}{\lambda_k}\right|\frac{2}{\pi}\left|\int_0^t\int_0^\pi \tilde{\theta}(\tau)f(\zeta,\tau,\tilde{\omega})\sin 2k\zeta\sin\tilde{\lambda}_k(t-\tau)d\zeta d\tau\right| \\
&+\sum_{k=1}^{\infty}\frac{1}{\lambda_k}\frac{2}{\pi}\left|\int_0^t\int_0^\pi \left[\tilde{\theta}(\tau)-\theta(\tau)\right]f(\zeta,\tau,\tilde{\omega})\sin 2k\zeta\sin\lambda_k(t-\tau)d\zeta d\tau\right| \\
&+\sum_{k=1}^{\infty}\frac{1}{\lambda_k}\frac{2}{\pi}\left|\int_0^t\int_0^\pi \tilde{\theta}(\tau)\left[f(\zeta,\tau,\tilde{\omega})-f(\zeta,\tau,\omega)\right]\sin 2k\zeta\sin\lambda_k(t-\tau)d\zeta d\tau\right| \\
&+\sum_{k=1}^{\infty}\frac{1}{\lambda_k}\int_0^t\left(\frac{2}{\pi}\left|\int_0^\pi \tilde{\theta}(\tau)f(\zeta,\tau,\tilde{\omega})\sin 2k\zeta d\zeta\right|\right)\left|\sin\tilde{\lambda}_k(t-\tau)-\sin\lambda_k(t-\tau)\right| d\tau.
\end{aligned}
$$

The statements $\left|\tilde{E}''(t)-E''(t)\right|$, $\left|\frac{1}{\lambda_k}-\frac{1}{\tilde{\lambda}_k}\right|$, $\left|\sin\lambda_k t-b_k\sin\tilde{\lambda}_k t\right|$, $\left|\cos\lambda_k t-a_k\cos\tilde{\lambda}_k t\right|$, $\left|\sin\lambda_k(t-\tau)-\sin\tilde{\lambda}_k(t-\tau)\right|$ in the inequality (15) are bounded for k, τ and t $(0\le\tau\le t\le T)$ as $\varepsilon\to 0$. Let us denote all of these statements by $\sigma(\varepsilon)$ and we rewrite (15) as follow

$$
\begin{aligned}
|\tilde{\omega}(t,\varepsilon)-\tilde{\omega}(t)| \le \sigma(\varepsilon) &+ \frac{1}{\pi}\left|\int_0^t\int_0^\pi [\tilde{\theta}(\tau)-\theta(\tau)](t-\tau)f(\zeta,\tau,\omega)d\zeta d\tau\right| \\
&+ \frac{1}{\pi}\left|\int_0^t\int_0^\pi \tilde{\theta}(\tau)(t-\tau)\left[f(\zeta,\tau,\tilde{\omega})-f(\zeta,\tau,\omega)\right]d\zeta d\tau\right| \\
&+ \sum_{k=1}^{\infty}\frac{1}{\lambda_k}\frac{2}{\pi}\left|\int_0^t\int_0^\pi \left[\tilde{\theta}(\tau)-\theta(\tau)\right]f(\zeta,\tau,\tilde{\omega})\cos 2k\zeta\sin\lambda_k(t-\tau)d\zeta d\tau\right| \\
&+ \sum_{k=1}^{\infty}\frac{1}{\lambda_k}\frac{2}{\pi}\left|\int_0^t\int_0^\pi \left[\tilde{\theta}(\tau)-\theta(\tau)\right]f(\zeta,\tau,\tilde{\omega})\sin 2k\zeta\sin\lambda_k(t-\tau)d\zeta d\tau\right| \\
&+ \sum_{k=1}^{\infty}\frac{1}{\lambda_k}\frac{2}{\pi}\left|\int_0^t\int_0^\pi \tilde{\theta}(\tau)\left[f(\zeta,\tau,\tilde{\omega})-f(\zeta,\tau,\omega)\right]\cos 2k\zeta\sin\lambda_k(t-\tau)d\zeta d\tau\right| \\
&+ \sum_{k=1}^{\infty}\frac{1}{\lambda_k}\frac{2}{\pi}\left|\int_0^t\int_0^\pi \tilde{\theta}(\tau)\left[f(\zeta,\tau,\tilde{\omega})-f(\zeta,\tau,\omega)\right]\sin 2k\zeta\sin\lambda_k(t-\tau)d\zeta d\tau\right|.
\end{aligned}
$$

By applying Cauchy, Bessel, Hölder inequalities, and Lipshitz condition to the last inequality, we have

$$
\begin{aligned}
&|\tilde{\omega}(t,\varepsilon)-\omega(t)| \le \sigma(\varepsilon) \qquad (16)\\
&+2\sqrt{\frac{t^3}{3\pi}}\left\{\left(\int_0^t\int_0^\pi\left\{\left|\tilde{\theta}(\tau)-\theta(\tau)\right|f(\xi,\tau,\omega)\right\}^2 d\xi d\tau\right)^{\frac{1}{2}}+\left(\int_0^t\int_0^\pi\left\{\tilde{\theta}(\tau)b(\xi,\tau)\left|\tilde{\omega}-\omega\right|\right\}^2 d\xi d\tau\right)^{\frac{1}{2}}\right\}\\
&+2\sqrt{\frac{\pi t}{6}}\left\{\left(\int_0^t\int_0^\pi\left\{\left|\tilde{\theta}(\tau)-\theta(\tau)\right|f(\xi,\tau,\tilde{\omega})\right\}^2 d\xi d\tau\right)^{\frac{1}{2}}+\left(\int_0^t\int_0^\pi\left\{\tilde{\theta}(\tau)b(\xi,\tau)\left|\tilde{\omega}-\omega\right|\right\}^2 d\xi d\tau\right)^{\frac{1}{2}}\right\}.
\end{aligned}
$$

Then we use the result of the difference of the inverse coefficients (14) in (16), we have

$$|\tilde{\omega}(t,\varepsilon)-\omega(t)| \leq \left(1+\frac{CM}{B}\right)\sigma(\varepsilon)+\left(\frac{2CM}{BM_*}\sqrt{\frac{t}{6\pi}}+C\right)\left(\int_0^t\int_0^\pi \left\{\tilde{\theta}(\tau)b(\zeta,\tau)\,|\tilde{\omega}-\omega|\right\}^2 d\zeta d\tau\right)^{\frac{1}{2}},$$

$$C=\left(2\sqrt{\frac{t^3}{3\pi}}+2\sqrt{\frac{\pi t}{6}}\right).$$

If we take into account the inequality $(y+z)^2 \leq 2y^2+2z^2$, then

$$|\tilde{\omega}(t,\varepsilon)-\omega(t)|^2 \leq 2\left(1+\frac{CM}{B}\right)^2\sigma^2(\varepsilon) +2\left(\frac{2CM}{BM_*}\sqrt{\frac{t}{6\pi}}+C\right)^2\left(\int_0^t\int_0^\pi \left\{\tilde{\theta}(\tau)b(\zeta,\tau)\,|\tilde{\omega}-\omega|\right\}^2 d\zeta d\tau\right).$$

Finally, applying Gronwall inequality to the last inequality, we have

$$|\tilde{\omega}(t,\varepsilon)-\omega(t)|^2 \leq 2\left(1+\frac{CM}{B}\right)^2\sigma^2(\varepsilon) \times \exp\left\{2\left(\frac{2CM}{BM_*}\sqrt{\frac{t}{6\pi}}+C\right)^2\left(\int_0^t\int_0^\pi \left\{\tilde{\theta}(\tau)b(\zeta,\tau)\right\}^2 d\zeta d\tau\right)\right\}. \tag{17}$$

Thus, the right-hand side of (17) converges to zero as ε approaches to zero. That is,

$$\lim_{\varepsilon\to 0}\tilde{\omega}(t,\varepsilon)=\omega(t).$$

In a previous study, we looked at solutions to the problems (1)-(4) and (5)-(8) in cases $\varepsilon>0$ and $\varepsilon=0$, respectively. This paper investigated the convergence of the solution (9) to the solution (11) as $\varepsilon\to 0$ under the theorem conditions. The solution was therefore found to be

$$\lim_{\varepsilon\to 0}\tilde{\omega}(x,t,\varepsilon)=\omega(x,t).$$

□

4. Numerical Method

The Finite Difference Method is commonly used for solving the wave equation due to its simplicity and efficiency. It approximates derivatives using straightforward difference formulas, which is ideal for handling the second-order partial

derivatives in the wave equation. Additionally, The Finite Difference Method is computationally efficient, especially for problems on structured grids, making them less resource-intensive than more complex methods like Finite Element or Spectral Methods.

We devise an iterative algorithm aimed at the linearizing the problem.

$$\frac{\partial^2 \omega^{(n)}}{\partial t^2} = \varepsilon \frac{\partial^4 \omega^{(n)}}{\partial x^2 \partial t^2} + \frac{\partial^2 \omega^{(n)}}{\partial x^2} + \theta(t) f\left(x, t, \omega^{(n-1)}\right), \tag{18}$$

$$\begin{aligned} \omega^{(n)}(x,0) &= \chi(x), \ x \in [0,\pi], \\ \omega_t^{(n)}(x,0) &= \phi(x), \ x \in [0,\pi] \ , \end{aligned} \tag{19}$$

$$\begin{aligned} \omega^{(n)}(0,t) &= \omega^{(n)}(\pi,t), \quad t \in [0,T], \\ \omega_x^{(n)}(0,t) &= \omega_x^{(n)}(\pi,t), \ t \in [0,T]. \end{aligned} \tag{20}$$

By setting $\omega^{(n)}(x,t) = v(x,t)$ and $f\left(x,t,\omega^{(n-1)}\right) = \tilde{f}(x,t)$, we can express the problem Eqs. (18)-(20) as a linear problem.

$$\frac{\partial^2 v}{\partial t^2} = \varepsilon \frac{\partial^4 v}{\partial x^2 \partial t^2} + \frac{\partial^2 v}{\partial x^2} + \theta(t) \tilde{f}(x,t), \ (x,t) \in D. \tag{21}$$

After the linearization method, implicit finite difference scheme is applied to solve the problem numerically. In Eq. (22), a second-order accurate backward finite difference scheme was used for temporal discretization. For the term with epsilon and last term in the same equation, a fourth-order accurate central differencing scheme was employed.

$$\begin{aligned} &\frac{1}{\Delta t^2}\left(2v_i^{j+3} - 5v_i^{j+2} + 4v_i^{j+1} - v_i^j\right) \\ &\quad = \frac{\varepsilon}{16\Delta x^2 \Delta t^2}\left[\left(v_{i+2}^{j+3} - 2v_i^{j+3} + v_{i-2}^{j+3}\right) - \left(2v_{i+2}^{j+1} - 4v_i^{j+1} + 2v_{i-2}^{j+1}\right)\right] \\ &\quad + \frac{\varepsilon}{16\Delta x^2 \Delta t^2}\left(v_{i+2}^{j-1} - 2v_i^{j-1} + v_{i-1}^{j-1}\right) \\ &\quad + \frac{1}{12\Delta x^2}\left(v_{i+2}^{j+3} + 16v_{i+1}^{j+3} - 30v_i^{j+3} + 16v_{i-1}^{j+3} - v_{i-2}^{j+3}\right) + s^{j+2}\tilde{f}^{j+2}. \end{aligned} \tag{22}$$

Initial condition is defined as

$$v_i^0 = \varphi_i. \tag{23}$$

Periodic boundary condition is combination of Dirichlet and Neumann boundary conditions, and it is defined as

$$v_1^j = v_{Nx}^j, \tag{24}$$

$$v_{Nx}^j = \frac{v_2^j + v_{Nx-1}^j}{2}. \tag{25}$$

The computational domain spans $[0,\pi]$ in the x-direction and $[0,T]$ in time. It's discretized into intervals such that $x_i = i\,(\Delta x - 1)$ for $i = 1, 2, ..., Nx$ in space, and $t_j = j\Delta t$ for $j = 1, 2, ..., Nt$ in time. Here Δx represents the spatial increment, calculated as π/Nx and Δt represents the time step, calculated as T/Nt Nx and Nt are two positive integers. The values v, φ and f are discretized as $v_i^j = v\,(x_i, t_j)\,, \varphi_i = \varphi\,(x_i)$ and $\tilde{f}^{j+2} = f\,(x_i, t_{j+2})$, respectively. The initial time $t = 0$ denotes the initial condition. In our numerical computation $j+3$ represents the present time, $j+2$ denotes the time just before the present, $j+1$ represents the two steps before the present, and j three steps before the present.

To determine the inverse coefficient $\theta\,(t)$, we integrate Eq. (1) over the range from 0 to φ with respect to x, while incorporating Eq. (3) and Eq. (4), leading to

$$\theta\,(t) = \frac{E''\,(t) - \varepsilon\,[\pi v_{xtt}\,(\pi,t) - v_{tt}\,(\pi) + v_{tt}\,(0)] - \pi v_x\,(\pi,t)}{\int\limits_0^\pi x\tilde{f}\,(x,t)\,dx}. \tag{26}$$

The individual discretization of the elements constituting Eq. (26) using finite differences one by

$$E''\,(t) = \left[\left(2E^{j+2} - 5E^{j+1} + 4E^j - E^{j-1}\right)/\Delta t^2\,\right], \tag{27}$$

$$v_{tt}\,(\pi) = \left(\left(2v_{Nx}^{j+2} - 5v_{Nx}^{j+1} + 4v_{Nx}^j - v_{Nx}^j\right)/\Delta t^2\,\right), \tag{28}$$

$$v_{tt}\,(0) = \left(\left(2v_1^{j+2} - 5v_1^{j+1} + 4v_1^j - v_1^j\right)/\Delta t^2\,\right), \tag{29}$$

$$\pi v_x\,(\pi,t) = \pi\left(3v_{Nx}^{j+2} - 4v_{Nx-1}^{j+2} + 4v_{Nx-2}^{j+2}\right)/2\Delta x\,, \tag{30}$$

$$\pi v_{xtt}\,(\pi,t) = \pi\left(\left(\left(v_{i+1}^{j+2} - 2v_{i+1}^{j+1} + v_{i+1}^j\right) - \left(v_i^{j+2} - 2v_i^{j+1} + v_i^j\right)\right)/\Delta x\Delta t^2\,\right). \tag{31}$$

Second-order accurate backward finite difference schemes have been used for Eqs. (27)-(30). The mixed derivative used in Eq. (31) is discretized using a first-order accurate backward finite difference method.

$$\left(\tilde{f}in\right)^{j+2} = \int\limits_0^\pi x\tilde{f}\,(x,t)\,dx. \tag{32}$$

Trapezoidal rule for integration is employed to compute Eq. (30). The value of Nx utilized for numerical solutions differs from the value of Nin used for the trapezoidal rule integration.

When computing the inverse coefficient during the initial time steps, we utilize the initial value of v , yet we refrain from presenting the detailed discretization here to avoid excessive elaboration.

For the numerical solution of Eq. (22), no iterative methods were employed, a direct method was used instead. The right-hand side matrix constitutes from

previous values, and it is used in direct method. The right-hand side matrix

$$rhs_i = -5u_i^{j+2} + 4u_i^{j+1} - u_i^j + \frac{\varepsilon}{8\Delta x^2}\left(u_{i+2}^{j+1} - 2u_i^{j+1} + u_{i-2}^{j+1}\right) - \frac{\varepsilon}{16\Delta x^2}\left(u_{i+2}^{j-1} - 2u_i^{j-1} - u_{i-2}^{j-1}\right) - s^{j+2}\widetilde{f}^{j+2}\Delta t^2. \tag{33}$$

5. Numerical Example

Considering inverse problem

$$f(x,t,\omega) = \varepsilon^2 + \left(4 + 4\varepsilon^3 + \varepsilon^2\right)\sin(2x),$$

$$\varphi(x) = 1 + \sin 2x, E(t) = \frac{\left(\pi^2 - \pi\right)}{2}e^{\varepsilon t}, x \in [0,\pi], t \in [0,T].$$

In that case, the problem transforms as

$$\omega_{tt} - \varepsilon\omega_{xxtt} - \omega_{xx} = \theta(t)\sin(2x)\left[\varepsilon^2 + \left(4 + 4\varepsilon^3 + \varepsilon^2\right)\sin(2x)\right]$$

$$\omega(x,0) = 1 + \sin 2x,\ x \in [0,\pi],$$

$$\omega(0,t) = \omega(\pi,t),\ \omega_x(0,t) = \omega_x(\pi,t),\ 0 \le t \le T,$$

$$\int_0^\pi x\omega(x,t)dx = \frac{\left(\pi^2 - \pi\right)}{2}e^{\varepsilon t}.$$

The analytical solution of this problem can be defined as

$$\{\theta(t), \omega(x,t)\} = \left\{e^{\varepsilon t}, (1 + \sin(2x))\, e^{\varepsilon t}\right\}.$$

5.1. **Grid Independence Study, Time Step Size Determination and Validation.** Since the variation of ω over time becomes more significant for the $\varepsilon = 2$, grid independence, time step size determination, and validation studies were conducted for the $\varepsilon = 2$ case. For the grid independence study, seven different grid densities are used, these are 20, 40, 80, 160, 320, 640 and 1280. The grid independence study is repeated for five different time steps. The time steps used are in descending order: 0.01s, 0.005s, 0.0025s, 0.00125s, and 0.000625s. The grid independence studies for each time step are illustrated in Figure 1. The ω values shown in grid independence study are the maximum ω values at 1sn. The results estimated with 640 grids for all time steps are very close to those estimated with 1280 grids. Therefore, the grid number of 640 is determined as the grid independent mesh.

For the ε value of 2, the determination of the time step size for the grid independent mesh number of 640 grid is shown in Figure 2. Similarly, the ω values shown in the time step size determination study are the maximum ω values at 1s. It is observed that the omega value increases linearly, as the time step size decreases. However, it can be seen that the ω prediction for the time step sizes of 0.00125s and 0.000625s are close the each other. Therefore, the appropriate time step is

determined to be 0.00125s. The result in the subsequent validation study is based on the numerical solution with 640 grid numbers and a time step size of 0.00125s.

As previously mentioned, numerical solutions are obtained by selecting 640 grid number and a time step size of 0.00125s based on the grid independence and time step size determination study. The obtained numerical solutions are compared and validated against the exact solutions. The validation study is conducted for the ε value of 2. The validation of the inverse coefficient is shown in Figure 3. In Figure 3(a), the time-dependent variation of the inverse coefficient is given as both numerical and exact solutions. Due to the exponential nature with time, the inverse coefficient increases, and the real solutions closely match the numerical solutions.

In Figure 3(b), the time-dependent variation of the real errors is observed. The real errors increase with time, although these real errors are very small. Finally, to better compare the real solution with the numerical solution, the absolute relative true error is given as a function of time in Figure 3(c). The absolute relative true errors exhibit oscillations over time, but these oscillations are on a very small scale. Overall, the average absolute relative real error is at the level of 0.192%, indicating the numerical solution for the inverse coefficient.

The validation of the omega value for $\varepsilon = 2$ is shown in Figure 4. In Figure 4(a), the numerical prediction of ω is depicted, in Figure 4(b), the values of ω obtained from the analytical solution are shown, and in Figure 4(c), the true error between these two solutions is presented as a function of time. Upon inspection of Figures 4(a) and (b), it can be observed that there is little difference between the numerical solution and the analytical solution. To better compare the two cases, the true error between the two solutions is examined, revealing that the error is minimal at the initial times and increases with time, particularly in boundary regions. However, despite this increase, the resulting real error is at the level of 0.04. This indicates that the numerical solution has been validated.

5.2. **Numerical Predictions.** After the grid independence, timed step size determination and validation studies, it has been decided to use 640 grids and time step size of 0.00125s in subsequent numerical computations. Now, numerical solutions have been computed and compared at specific interval of 0.5 ranging from $\varepsilon = 0$ to $\varepsilon = 3$.

In Figure 5, the numerical prediction of the inverse coefficients for all epsilon values is shown. The inverse coefficient is an exponential function, becoming more prominent as epsilon increases. While at zero seconds, the exponential function-based inverse coefficient takes a constant value of unity for all epsilons, its value increases as time progresses.

Figure 6 depicts the variations of ω values for all ε values considered at (a)0.5s and (b)1s. These ω values are obtained from numerical predictions. The general trend of omega values increases for all ε values from the beginning of the domain to a length of 0.79 and then decreases to approximately 2.36 length until reaching zero, after which it tends to increase again until the end of the domain. While

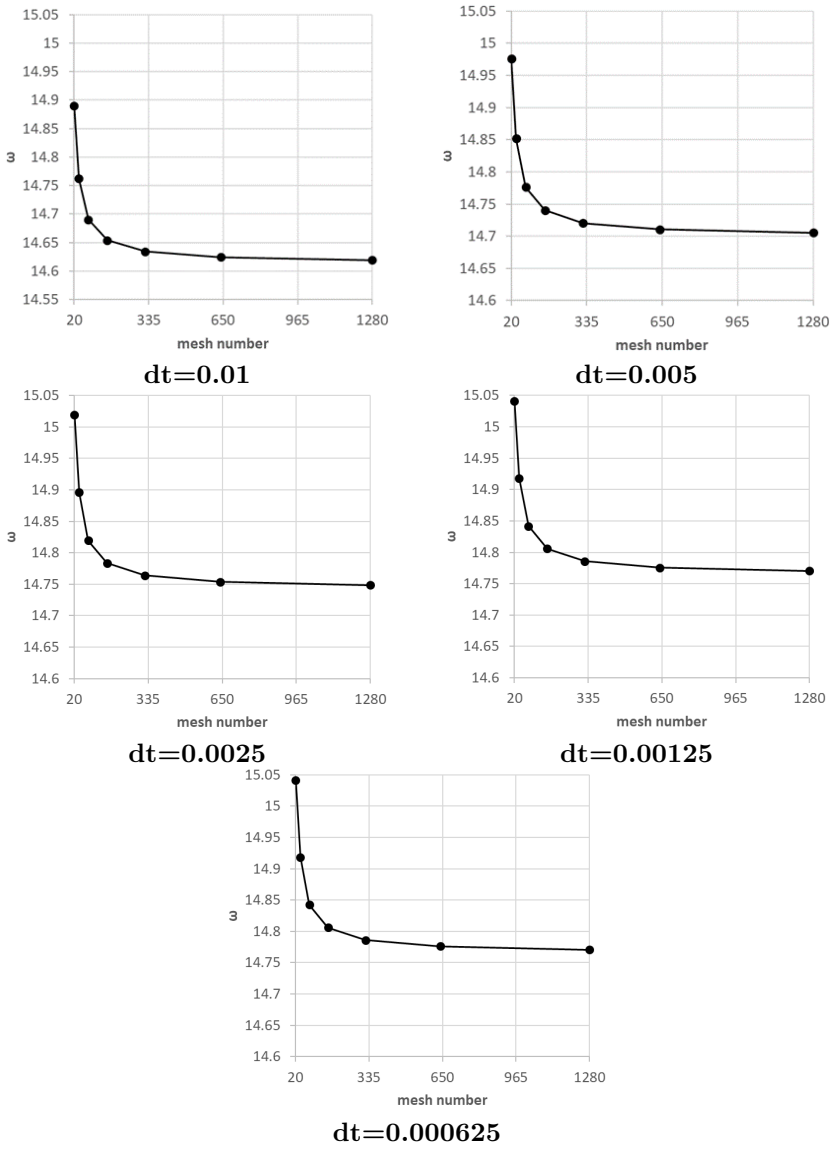

FIGURE 1. Grid independence study for $\varepsilon = 2$

the ω value obtained at $\varepsilon = 0$ is symmetric, symmetry is disrupted as ε increases. Moreover, ω values increase with both ε and time. At $t = 0.5s$, the maximum ω value for $\varepsilon = 3$ is around 9, whereas at $t = 1s$, the maximum ω value for $\varepsilon = 3$ is

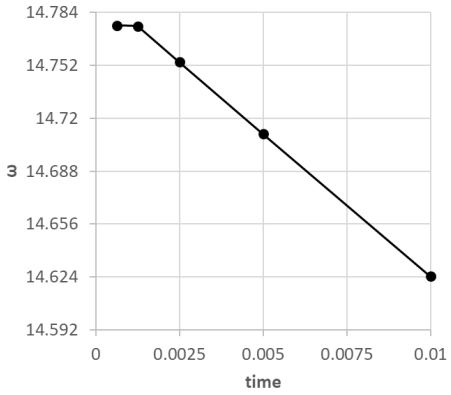

FIGURE 2. Time step size determination for $\varepsilon = 2$

approximately 40. Additionally, at $t = 1s$, when $\varepsilon = 2.5$, the maximum ω value is around 24, while it reaches approximately 41 when $\varepsilon = 3$, as mentioned earlier.

Figure 7 presents three-dimensional graphs showing the variation of ω values predicted from numerical solutions with respect to both length and time for (a) $\varepsilon = 0$, (b) $\varepsilon = 0.5$, (c) $\varepsilon = 1$, (d) $\varepsilon = 1.5$, (e) $\varepsilon = 2$, (f) $\varepsilon = 2.5$, and (g) $\varepsilon = 3$. Figure 7 transforms the lines obtained from only two times (0.5s and 1s) mentioned in Figure 6 into area plots showing all times. To ensure better comparison across all values, all graphs are drawn on the same scale. All interpretations made in Figure 6 can also be applied to Figure 7.

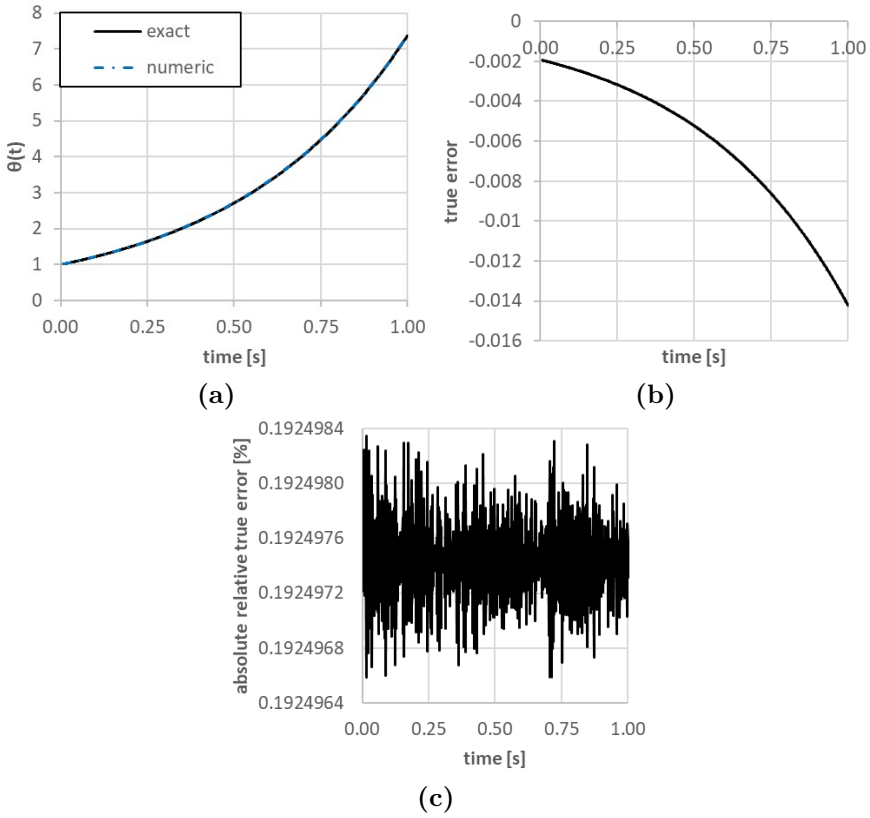

FIGURE 3. Validation of inverse coefficient for $\varepsilon = 2$

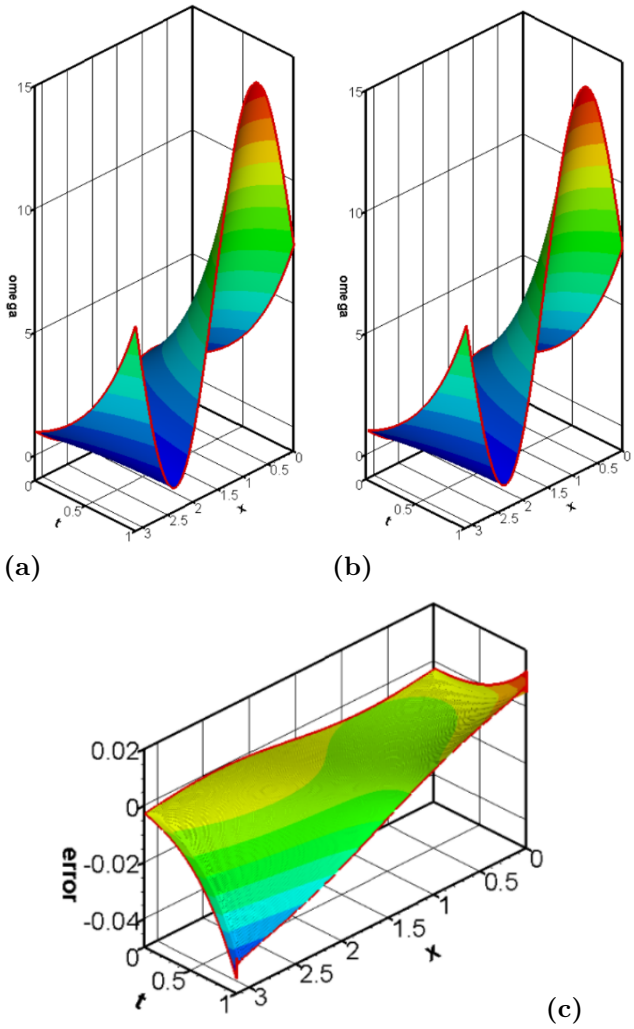

FIGURE 4. Validation of ω for $\varepsilon = 2$

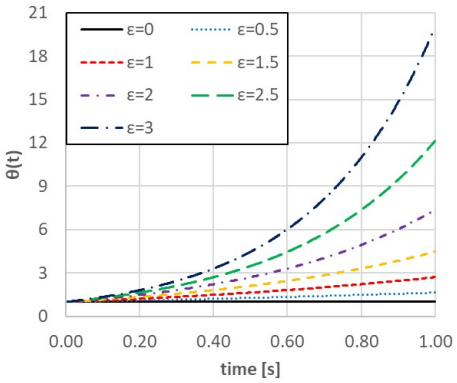

FIGURE 5. Numerical predictions of inverse coefficient for all ε

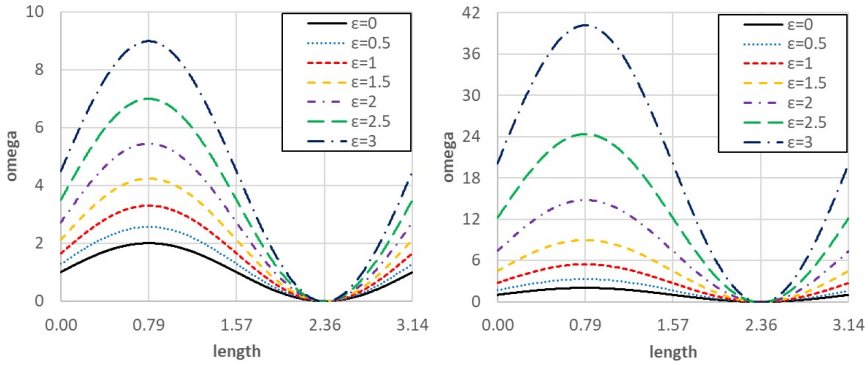

FIGURE 6. Numerical predictions of ω for all ε at(a) $t = 0.5s$ and (b)$t = 1s$

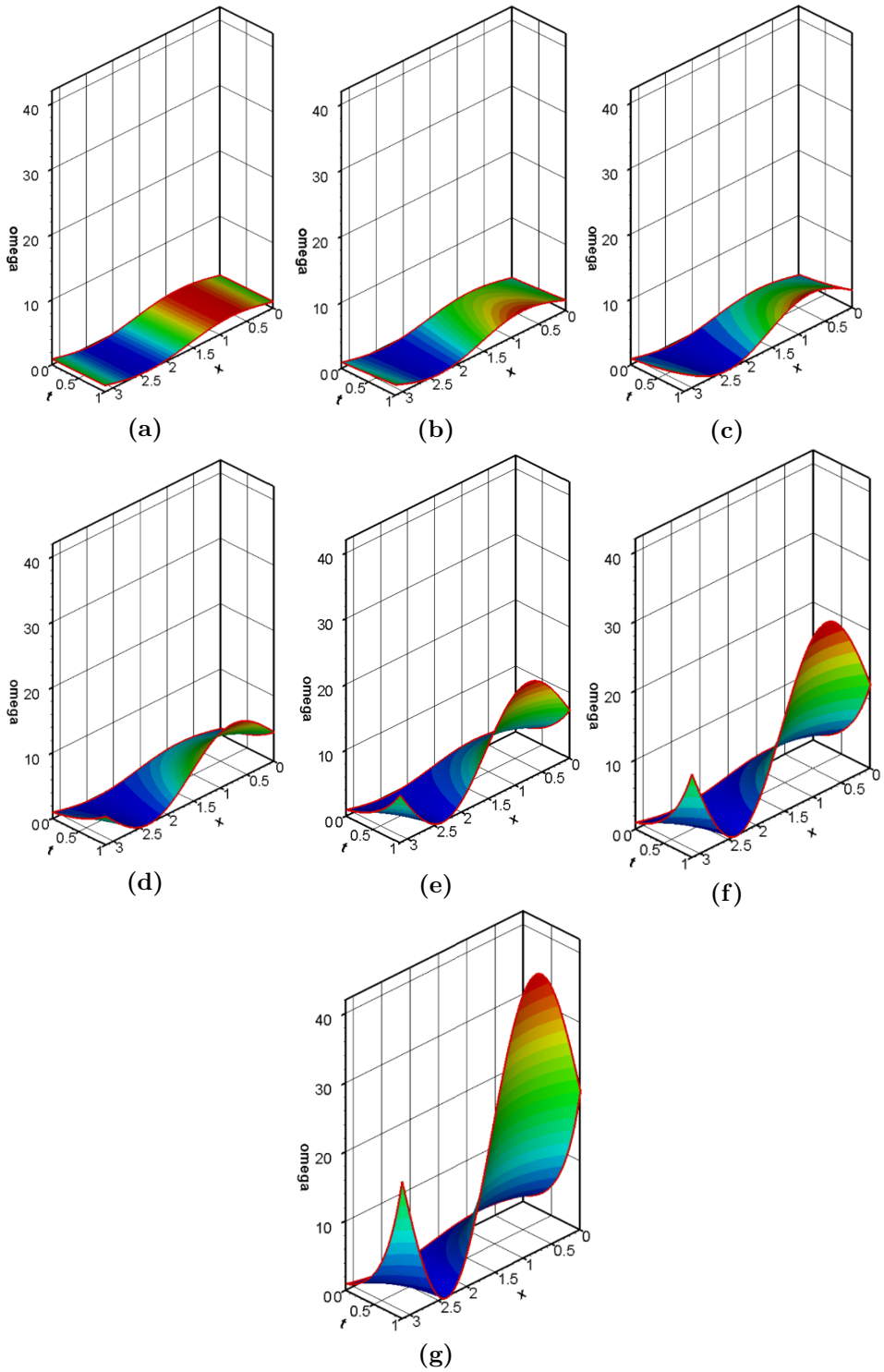

FIGURE 7. Numerical predictions of ω at all times and for (a)$\varepsilon = 0$, (b)$\varepsilon = 0.5$, (c)$\varepsilon = 1$, (d)$\varepsilon = 1.5$, (e)$\varepsilon = 2$, (f)$\varepsilon = 2.5$ and (g)$\varepsilon = 3$

6. Conclusions

Analytical and numerical investigation of one-dimensional nonlinear hyperbolic ($\varepsilon = 0$) and pseudo-hyperbolic ($\varepsilon \neq 0$) equation with periodic condition is done. This investigation contains an inverse problem of unknown unsteady coefficients. For analytical solution, the generalized Fourier method is utilized to calculate Fourier coefficients. Additionally, an iterative approach is employed to ensure convergence while assessing the uniqueness and stability of the solution for the nonlinear problem. For numerical solution, implicit finite difference equation with higher accurate schemes is applied. A second-order accurate time discretization is applied, and for the discretization of spatial and multi-variable partial differential equations, fourth-order accurate finite difference equations are implemented. The cases where ($\varepsilon = 0$) and $\varepsilon \neq 0$ (different epsilon values) have been solved analytically and numerically, and compared with each other. The main conclusions are listed below;

- In light of the grid independence and time step size determination study, 640 mesh number and 0.00125s time step size are determined. Using this mesh number and time step size, the numerical computation for the $\varepsilon = 2$ is validated against analytical results for both ω and inverse coefficient.
- In the case of $\varepsilon = 0$, the inverse coefficient does not vary with time ($\theta(t) = 1$), however, as ε and time increases, the inverse coefficient increases due to its exponential nature.
- The distribution of ω over length is symmetric at a certain time in the case of hyperbolic equation ($\varepsilon = 0$), but in the case of pseudo-hyperbolic equation ($\varepsilon \neq 0$) the distribution of ω over length is asymmetric.
- Due to periodic boundary conditions, the ω values at the boundaries of the solution domain are identical to each other, and as the ε value increases, the ω values at the boundary points also increase.
- As the time and ε value increase, the magnitude of ω oscillations increase at especially at the beginning of the solution domain.

Author Contribution Statements All authors contributed equally and significantly in writing this article. All authors read and approved the final manuscript.

Declaration of Competing Interests This work does not have any conflict of interest.

References

[1] Afshar, S., Soltanalizadeh, B., Solution of the two-dimensional second-order diffusion equation with nonlocal boundary condition, *Int. J. Pure Appl. Math*, 94(2) (2014), 119-131. http://dx.doi.org/10.12732/ijpam.v94i2.1

[2] Antunes, A. J., Leal-Toledo, R. C., da Silveira Filho, O. T., Toledo, E. M., Finite difference method for solving acoustic wave equation using locally adjustable time-steps, *Procedia Computer Science*, 29 (2014), 627-636. https://doi.org/10.1016/j.procs.2014.05.056

[3] Aslan, E., Taymaz, I., Çakir, K., Kahveci, E. E., Numerical and experimental investigation of tube bundle heat exchanger arrangement effect on heat transfer performance in turbulent flows, *Isı Bilimi ve Tekniği Dergisi*, 43(2) (2023), 175-190. https://doi.org/10.47480/isibted.1391408

[4] Aslan, E., Numerical investigation of the heat transfer and pressure drop on tube bundle support plates for inline and staggered arrangements, *Progress in Computational Fluid Dynamics, an International Journal*, 16(1) (2016), 38-47. https://doi.org/10.1504/PCFD.2016.074249

[5] Baglan, I., Akdemir, A. O., Dokuyucu, M. A., Inverse coefficient problem for quasilinear pseudo-parabolic equation by Fourier method, *Filomat*, 37(21) (2023), 7217-7230. https://doi.org./10.2298/FIL2321217B

[6] Bağlan, İ., Canel, T., Analysis of inverse Euler-Bernoulli equation with periodic boundary conditions, *Turkish Journal of Science*, 7(3) (2022), 146-156.

[7] Bağlan, İ., Canel, T., Fourier method for higher order quasi-linear parabolic equation subject with periodic boundary conditions, *Turkish Journal of Science*, 6(3) (2021), 148-155.

[8] Baglan, I., Determination of a coefficient in a quasilinear parabolic equation with periodic boundary condition, *Inverse Problems in Science and Engineering*, 23(5) (2015), 884-900. https://doi.org/10.1080/17415977.2014.947479

[9] Bellassoued, M., Aïcha, I. B., An inverse problem of finding two time-dependent coefficients in second order hyperbolic equations from Dirichlet to Neumann map, *Journal of Mathematical Analysis and Applications*, 475(2) (2019), 1658-1684. https://doi.org/10.1016/j.jmaa.2019.03.038

[10] Benim, A. C., Diederich, M., Pfeiffelmann, B., Aerodynamic optimization of airfoil profiles for small horizontal axis wind turbines, *Computation*, 6(2) (2018), 34. https://doi.org/10.3390/computation6020034

[11] Benim, A. C., Zinser, W. A., Segregated formulation of Navier-Stokes equations with finite elements, *Comput. Methods Appl. Mech. Engineering*, 57 (1986), 223-237. https://doi.org/10.1016/0045-7825(86)90015-0

[12] Benim, A. C., Zinser, W., Investigation into the finite element analysis of confined turbulent flows using a $k-\epsilon$ model of turbulence, *Computer Methods in Applied Mechanics and Engineering*, 51(1-3) (1985), 507-523. https://doi.org/10.1016/0045-7825(85)90045-3

[13] Benim, A. C., Finite element analysis of confined turbulent swirling flows, *Int. J. Num. Meth. Fluids*, 11 (1990), 697-717. https://doi.org/10.1002/fld.1650110602

[14] Bhattacharyya, S., Benim, A. C., Chattopadhyay, H., Banerjee, A., Experimental and numerical analysis of forced convection in a twisted tube, *Thermal Science*, 23 (2019), 1043–1052. https://doi.org/10.2298/TSCI19S4043B

[15] Bhattacharyya, S., Benim, A. C., Pathak, M., Chamoli, S., Gupta, A., Thermohydraulic characteristics of inline and staggered angular cut baffle inserts in the turbulent flow regime, *Journal of Thermal Analysis and Calorimetry*, 140 (2020), 1519–1536. https://doi.org/10.1007/s10973-019-09094-8

[16] Biswas, N., Manna, N. K., Datta, A., Mandal, D. K., Benim, A. C., Role of aspiration to enhance MHD convection in protruded heater cavity, *Progress in Computational Fluid Dynamics, an International Journal*, 20(6) (2020), 363-378. https://doi.org/10.1504/PCFD.2020.111408

[17] Cao, Y., Yin, J., Wang, C., Cauchy problems of semilinear pseudo-parabolic equations, *Journal of Differential Equations*, 246(12) (2009), 4568-4590. https://doi.org/10.1016/j.jde.2009.03.021

[18] Ciftci, I., Halilov, H., Dependency of the solution of quasilinear pseudo-parabolic equation with periodic boundary condition on ϵ, *Int. Journal of Math. Analysis*, 2(18) (2008), 881–888.
[19] Courant, R., Hilbert, D., Methods of Mathematical Physics: Partial Differential Equations, John Wiley & Sons, 2008.
[20] Damseh, R. A., Tahat, M. S. and Benim, A. C., Nonsimilar solutions of magnetohydrody-namic and thermophoresis particle deposition on mixed convection problem in porous media along a vertical surface with variable wall temperature,*Progress in Computational Fluid Dynamics, an International Journal*, 9(1) (2009), 58-65. https://doi.org/10.1504/PCFD.2009.022309
[21] Dimova, M., Kolkovska, N., Kutev, N., Global behavior of the solutions to nonlinear wave equations with combined power-type nonlinearities with variable coefficients, *Nonlinear Analysis*, 242 (2024), 113504. https://doi.org/10.1016/j.na.2024.113504
[22] Djidjeli, K., Price, W. G., Twizell, E. H., Wang, Y., Numerical methods for the solution of the third and fifth-order dispersive Korteweg-de Vries equations, *Journal of Computational and Applied Mathematics*, 58(3) (1995), 307-336. https://doi.org/10.1016/0377-0427(94)00005-L
[23] Dmitriev, V. G., Danilin, A. N., Popova, A. R., Pshenichnova, N. V., Numerical analysis of deformation characteristics of elastic inhomogeneous rotational shells at arbitrary displacements and rotation angles, *Computation*, 10(10) (2022), 184. https://doi.org/10.3390/computation10100184
[24] Evans, L. C., Partial Differential Equations, 2nd ed., American Mathematical Society, CA, 2022.
[25] Floridia, G., Takase, H., Inverse problems for first-order hyperbolic equations with time-dependent coefficients, *Journal of Differential Equations*, 305 (2021), 45-71. https://doi.org/10.1016/j.jde.2021.10.007
[26] Halilov, H., Güler, B. O., Kutlu, K., Dependency of the solution of a class of quartic partial differential quasilinear equation with periodic boundary condition on ε, *Gen*, 28(1) (2015), 59-71.
[27] Huang, M., Wang, Y., Shao, Z., Piston problem for the generalized Chaplygin Euler equations of compressible fluid flow, *Chinese Journal of Physics*, (2023). https://doi.org/10.1016/j.cjph.2023.08.015
[28] Ionkin, N. I., The solution of a certain boundary value problem of the theory of heat conduction with a nonclassical boundary condition, *Differentsial'nye Uravneniya*, 13(2) (1977), 294-304.
[29] Katbeh, J., Masad, E., Roja, K. L., Srinivasa, A., A framework for the analysis of dam-age and healing viscoelastic behaviour of asphalt binders, *Construction and Building Materials*, 374 (2023), 130908. https://doi.org/10.1016/j.conbuildmat.2023.130908
[30] Kostin, I., Panasenko, G., Khokhlov–Zabolotskaya–Kuznetsov type equation: nonlinear acoustics in heterogeneous media. Comptes rendus, *Mécanique*, 334(4) (2006), 220-224. DOI: 10.1016/j.crme.2006.01.010
[31] Liu, S., Triggiani, R., Global uniqueness and stability in determining the damping and potential coefficients of an inverse hyperbolic problem, *Nonlinear Analysis: Real World Applications*, 12(3) (2011), 1562-1590. https://doi.org/10.1016/j.nonrwa.2010.10.014
[32] Mehraliyev, Y. T., Ramazanova, A. T., Huntul, M. J., An inverse boundary value problem for a two-dimensional pseudo-parabolic equation of third order, *Results in Applied Mathematics*, 14 (2022), 100274. https://doi.org/10.1016/j.rinam.2022.100274
[33] Shu, T., Yang, K., Liu, Y., Feng, B., Wu, C., Wave-equation traveltime slope inversion by combining finite difference and crosscorrelation methods, *Journal of Applied Geophysics*, 206 (2022), 104817. https://doi.org/10.1016/j.jappgeo.2022.104817
[34] Smith, G. D., Numerical Solution of Partial Differential Equations: Finite Difference Methods, Oxford University Press, 1985.

[35] Song, J., Zhong, M., Karniadakis, G. E., Yan, Z., Two-stage initial-value iterative physics-informed neural networks for simulating solitary waves of nonlinear wave equations, *Journal of Computational Physics*, 505 (2024), 112917. https://doi.org/10.1016/j.jcp.2024.112917

[36] Versteeg, H. K., Malalasekera, W., An Introduction to Computational Fluid Dynamics, 2nd ed. Pearson Prentice Hall, London, 2007.

[37] Xia, J. L., Smith, B. L., Benim, A. C., Schmidli, J., Yadigaroglu, G., Effect of inlet and outlet boundary conditions on swirling flows, *Computers & Fluids*, 26 (1997), 811–823. https://doi.org/10.1016/S0045-7930(97)00026-1

[38] Xu, J., Xie, S., Fu, H., A two-grid block-centered finite difference method for the nonlinear regularized long wave equation, *Applied Numerical Mathematics*, 171 (2022), 128-148. https://doi.org/10.1016/j.apnum.2021.08.008

[39] Zhang, Y., Pang, Y., Wang, J., Concentration and cavitation in the vanishing pressure limit of solutions to the generalized Chaplygin Euler equations of compressible fluid flow, *European Journal of Mechanics-B/Fluids*, 78 (2019), 252-262. https://doi.org/10.1016/j.euromechflu.2019.103515